Frontiers of Information Technology & Electronic Engineering
www.jzus.zju.edu.cn; engineering.cae.cn; www.springerlink.com
ISSN 2095-9184 (print); ISSN 2095-9230 (online)
E-mail: jzus@zju.edu.cn

A general method of designing phase-shifting algorithms for grating lateral shearing interferometry*

Chao FANG[1,2], Yang XIANG[†‡1], Ke-qi QI[1,2]

[1]*State Key Laboratory of Applied Optics, Changchun Institute of Optics, Fine Mechanics and Physics, Chinese Academy of Sciences, Changchun 130033, China*

[2]*University of Chinese Academy of Sciences, Beijing 100039, China*

[†]E-mail: xiangy@sklao.ac.cn

Received Nov. 7, 2016; Revision accepted Nov. 28, 2016; Crosschecked June 8, 2018

Abstract: We propose a general method of designing phase-shifting algorithms for grating lateral shearing interferometry. The algorithms compensate for the zeroth-order effect error and phase-shifting error in varying degrees. We derive a general expression of the phase-shifting algorithm in grating lateral shearing interferometer and introduce the corresponding design method. Based on the expression and method, four phase-shifting algorithms are designed with different phase-shifting errors to obtain high measurement accuracy. A new 13-frame phase-shifting algorithm is designed and simulated with a large zeroth-order effect. Simulation results verify the general expression and the corresponding design method.

Key words: Interferometry; Phase measurement; Phase-shifting algorithms
https://doi.org/10.1631/FITEE.1601692 **CLC number:** O436

1 Introduction

The system wavefront aberration is one of the important parameters for evaluating a lithography projection lens, and has a fundamental impact on the critical dimension (Wang et al., 2006). There are several methods to measure the system wavefront aberration, such as point diffraction interferometry (Lee et al., 2000; Goldberg et al., 2004; Gao et al., 2010; Bai et al., 2013), lateral shearing interferometry (Takeda and Kobayashi, 1984; Schreiber and Schwider, 1997; Hasegawa M et al., 2004; Dai et al., 2016), and the Hartmann-Shack sensor (Fujii et al., 2003; Bueno et al., 2010; Li et al., 2015). Research shows that lateral shearing interferometry has great potential for improving the accuracy in system wavefront measurement (Miyakawa et al., 2009). The system wavefront of the projection lens is obtained by grating lateral shearing interferometer using the interferograms of the $\pm1^{st}$-order diffraction beams. However, in practice, there is still a certain percentage of the zeroth-order beam reaching the charge-coupled device (CCD) detector caused by manufacturing and assembly of the spatial filter (Hasegawa T et al., 2004; Zhu et al., 2007). The zeroth-order beam and the $\pm1^{st}$-order beams generate complicated interferograms, which increases the difficulty of wavefront restoration and reduces the accuracy of wavefront measurement. Therefore, it is significant to design special algorithms to suppress the zeroth-order effect and to compensate for the phase-shifting error. Zhu et al. (2004) proposed a 9-frame phase-shifting algorithm to eliminate the phase-shifting error and the zeroth-order effect. In 2013, we proposed an improved 11-frame phase-shifting algorithm that performed better with a large phase-shifting error

‡ Corresponding author

* Project supported by the National Science and Technology Major Project, China (No. 2009ZX02202005)

ORCID: Chao FANG, http://orcid.org/0000-0002-3880-2995

(Fang et al., 2013). In recent years, with the development and competition of projection lithography equipment, the need for accurate wavefront measurement of projection lens systems is obviously increasing. Based on the existing grating lateral shearing interferometer, new phase-restoration algorithms have been designed to improve the measurement accuracy of the wavefront of projection lens systems, which is significant in developing new lithography equipment with narrower critical dimension.

In this paper, we derive a general expression of a phase-shifting algorithm in a grating lateral shearing interferometer and introduce the corresponding design method. Based on the expression and method, a series of phase-shifting algorithms are designed to suppress the zeroth-order effect and phase-shifting error for a grating lateral shearing interferometer. Simulation results verify the expression and the corresponding method.

2 Principle

Fig. 1 shows a typical grating lateral shearing interferometer. The tested wavefront of W_0 is divided into several different wavefronts, W_0, $W_{\pm1}$, $W_{\pm2}$, …, by grating. With the spatial filter, only the $\pm1^{st}$-order and a certain percentage of the zeroth-order wavefronts go through the window and interfere with each other. The interferogram intensity I_0 is

$$I_0 = Q + V_1\cos\theta_1 + V_2\cos\theta_2 + V_3\cos\theta_3, \qquad (1)$$

where Q is a constant, V_1 is the visibility of the interferogram generated by the $+1^{st}$- and -1^{st}-order beams, V_2 is the visibility of the interferogram generated by the $+1^{st}$- and zeroth-order beams, V_3 is the visibility of interferogram generated by the zeroth- and -1^{st}-order beams, $\theta_1=2\pi(W_{+1}-W_{-1})/\lambda$ is the restoration phase to be tested, $\theta_2=2\pi(W_{+1}-W_0)/\lambda$ and $\theta_3=2\pi(W_0-W_{-1})/\lambda$ are phases to be eliminated, $W_{\pm1}(x, y)=W_0(x\pm\delta, y)$, and δ is the shearing ratio. At the grating in the interferometer, the designed $\pm1^{st}$-order diffraction efficiencies are 40%, so the zeroth-order diffraction efficiency is less than 20%. The amplitude of the zeroth-order beam going through a spatial filter is much smaller than those of the $\pm1^{st}$-order beams. So, V_2 and V_3 are much smaller than V_1.

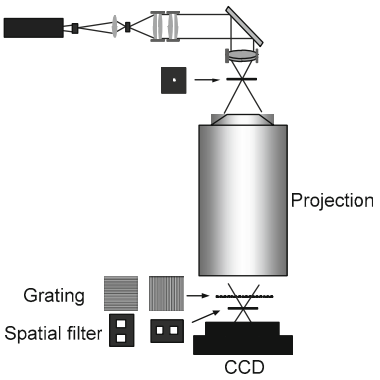

Fig. 1 Block diagram of a grating lateral shearing interferometer

The phase-shifting interference is achieved with grating and piezoelectric transducer (PZT). The interferogram intensity I_j for the j^{th} frame is

$$\begin{aligned} I_j = {} & Q + V_1\cos(\theta_1 + \phi_j) \\ & + V_2\cos(\theta_2 + \phi_j/2) + V_3\cos(\theta_3 + \phi_j/2), \end{aligned} \qquad (2)$$

where $\phi_j = j\pi/2+j\varepsilon$ is the amount of phase-shifting and ε is the phase-shifting error.

With an odd number of n frame interferograms, the restoration phase is derived as a general expression (Zhu and Gemma, 2001):

$$\tan\theta_1 = \frac{\sum_{j=0}^{2j+1<(n-1)/2} a_{2j+1}(I_{2j+1} - I_{-(2j+1)})}{\sum_{j=1}^{2j+1<(n-1)/2} a_{2j}(I_{2j} + I_{-2j}) - \sum_{j=1}^{2j+1<(n-1)/2} 2a_{2j}I_0}, \qquad (3)$$

where a_j is an unknown constant and we assume n=15.

Expand the numerator part of Eq. (3) in Taylor expansion form for the phase-shifting error ε, and omit the small quantity with high orders. A_1, containing terms θ_1 and Q in the numerator of Eq. (3), is

$$\begin{aligned} A_1 = {} & (\sin\theta_1)\Big[-2a_1 + 2a_7 + 2a_3 - 2a_5 \\ & + (-9a_3 + a_1 - 49a_7 + 25a_5)\varepsilon^2 \\ & + \left(-\frac{1}{12}a_1 + \frac{27}{4}a_3 - \frac{625}{12}a_5 + \frac{2401}{12}a_7\right)\varepsilon^4 \\ & + \left(\frac{1}{360}a_1 - \frac{81}{40}a_3 - \frac{3125}{72}a_5 - \frac{117649}{360}a_7\right)\varepsilon^6 \\ & + \left(\frac{729}{2240}a_3 - \frac{1}{20160}a_1 + \frac{823543}{2880}a_7 - \frac{78125}{4032}a_5\right)\varepsilon^8\Big]. \end{aligned} \qquad (4)$$

Similarly, A_2, containing term θ_2, can be expressed as

$$A_2=\frac{V_2}{V_1}(\sin\theta_2)\left[\sqrt{2}a_7+\sqrt{2}a_5-\sqrt{2}a_3-\sqrt{2}a_1+\left(\frac{3}{2}\sqrt{2}a_3+\frac{5}{2}\sqrt{2}a_5-\frac{7}{2}\sqrt{2}a_7-\frac{1}{2}\sqrt{2}a_1\right)\varepsilon+\left(-\frac{25}{8}\sqrt{2}a_5-\frac{49}{8}\sqrt{2}a_7+\frac{9}{8}\sqrt{2}a_3+\frac{1}{8}\sqrt{2}a_1\right)\varepsilon^2\right]. \tag{5}$$

A_3, containing term θ_3, can be expressed as

$$A_3=\frac{V_3}{V_1}(\sin\theta_3)\left[\sqrt{2}a_7+\sqrt{2}a_5-\sqrt{2}a_3-\sqrt{2}a_1+\left(\frac{3}{2}\sqrt{2}a_3+\frac{5}{2}\sqrt{2}a_5-\frac{7}{2}\sqrt{2}a_7-\frac{1}{2}\sqrt{2}a_1\right)\varepsilon+\left(-\frac{25}{8}\sqrt{2}a_5-\frac{49}{8}\sqrt{2}a_7+\frac{9}{8}\sqrt{2}a_3+\frac{1}{8}\sqrt{2}a_1\right)\varepsilon^2\right]. \tag{6}$$

Expand the denominator of Eq. (3) in Taylor expansion form for the phase-shifting error ε, and omit the small quantity with high orders. B_1, containing terms θ_1 and Q in the denominator of Eq. (3), can be expressed as

$$B_1=(\cos\theta_1)\left[(-4a_6-4a_2)+(36a_6-16a_4+4a_2)\varepsilon^2+\left(-108a_6+\frac{64}{3}a_4-\frac{4}{3}a_2\right)\varepsilon^4+\left(\frac{648}{5}a_6-\frac{512}{45}a_4+\frac{8}{45}a_2\right)\varepsilon^6+\left(-\frac{2916}{35}a_6+\frac{1024}{315}a_4-\frac{4}{315}a_2\right)\varepsilon^8\right]. \tag{7}$$

Similarly, B_2, containing term θ_2, can be expressed as

$$B_2=(V_2/V_1)(\cos\theta_2)[(-4a_4-2a_2-2a_6)+(6a_6-2a_2)\varepsilon+4a_4\varepsilon_2]. \tag{8}$$

B_3, containing term θ_3, can be expressed as

$$B_3=(V_3/V_1)(\cos\theta_3)[(-4a_4-2a_2-2a_6)+(6a_6-2a_2)\varepsilon+4a_4\varepsilon^2]. \tag{9}$$

3 Optimized algorithms focusing on the phase-shifting error

The phase-shifting error is the primary error to be compensated for, and the algorithm is also required to compensate for the zeroth-order effect. We should let the constant terms in A_2, A_3, B_2, and B_3 be zero, and omit the higher-order terms of ε. The phase-shifting error of ε is a small value. A_2 is approximately zero, because A_2 is the product of two small quantities (polynomial of ε and V_2/V_1). Similarly, A_3, B_2, and B_3 are approximately zeros. The conditions for determining unknown constants are

$$\sqrt{2}(a_7+a_5-a_3-a_1)=0, \tag{10}$$

$$-2(2a_4+a_2+a_6)=0. \tag{11}$$

3.1 Nine-frame phase-shifting algorithm

To suppress the phase-shifting error, letting the constant terms in A_1 equal those in B_1, we obtain

$$-2a_1+2a_7+2a_3-2a_5=-4a_6-4a_2. \tag{12}$$

When nine interferogram frames are used, we obtain a_1=1, a_5=0, a_6=0, and a_7=0. Letting the conditions of Eqs. (10)–(12) be satisfied, a_2=1, a_3=−1, and a_4=−1/2 are obtained. The 9-frame algorithm is

$$\tan\theta_1=\frac{2(I_3-I_{-3})-2(I_1-I_{-1})}{(I_4+I_{-4})-2(I_2+I_{-2})+2I_0}. \tag{13}$$

The phase-restoration error function $\Delta\theta_1$ of the 9-frame algorithm can be expressed as (Zhu et al., 2004)

$$\Delta\theta_1=\frac{\varepsilon^2}{4}\sin(2\theta_1). \tag{14}$$

3.2 Eleven-frame phase-shifting algorithm

To optimize the 11-frame algorithm, the conditions of the 9-frame algorithm are needed. Let the term of ε^2 in A_1 equal that in B_1. The new condition of unknown constants is

$$-9a_3+a_1-49a_7+25a_5=36a_6-16a_4+4a_2. \tag{15}$$

When 11 interferogram frames are used, we obtain a_1=1, a_6=0, and a_7=0. Here, we let the conditions of Eqs. (10)–(12) and (15) be satisfied. Therefore, we obtain a_2=1, a_3=−7/8, a_4=−1/2, and a_5=1/8. The 11-frame algorithm was proposed by us earlier (Fang et al., 2013):

$$\tan\theta_1=\frac{(I_5-I_{-5})-7(I_3-I_{-3})+8(I_1-I_{-1})}{-4(I_4+I_{-4})+8(I_2+I_{-2})-8I_0}. \quad (16)$$

The phase-restoration error function $\Delta\theta_1$ of the 11-frame algorithm is expressed as

$$\Delta\theta_1=\frac{\varepsilon^4}{16}\sin(2\theta_1). \quad (17)$$

3.3 Thirteen-frame phase-shifting algorithm

For a large phase-shifting error, the conditions of the 11-frame algorithm are required. Let the term of ε^4 in A_1 equal that in B_1. The new condition of unknown constants is

$$\begin{aligned}&-\frac{1}{12}a_1+\frac{27}{4}a_3-\frac{625}{12}a_5+\frac{2401}{12}a_7\\&=-108a_6+\frac{64}{3}a_4-\frac{4}{3}a_2.\end{aligned} \quad (18)$$

When 13 interferogram frames are used, we obtain a_1=1and a_7=0. Here, we let the conditions of Eqs. (10)–(12), (15), and (18) be satisfied. Therefore, we obtain a_2=31/32, a_3=−13/16, a_4=−1/2, a_5=3/16, and a_6=1/32. The 13-frame algorithm is

$$\tan\theta_1=\frac{32(I_1-I_{-1})-26(I_3-I_{-3})+6(I_5-I_{-5})}{31(I_2+I_{-2})-16(I_4+I_{-4})+(I_6+I_{-6})-32I_0}. \quad (19)$$

The phase-restoration error function $\Delta\theta_1$ of the 13-frame algorithm can be expressed as

$$\Delta\theta_1=\frac{\varepsilon^6}{64}\sin(2\theta_1). \quad (20)$$

3.4 Fifteen-frame phase-shifting algorithm

For a large phase-shifting error, the conditions of the 13-frame algorithm are required. Let the term of ε^6 in A_1 equal that in B_1. The new condition of unknown constants is

$$\begin{aligned}&\frac{1}{360}a_1-\frac{81}{40}a_3+\frac{3125}{72}a_5-\frac{117649}{360}a_7\\&=\frac{648}{5}a_6-\frac{512}{45}a_4+\frac{8}{45}a_2.\end{aligned} \quad (21)$$

When 15 interferogram frames are used, we obtain a_1=1 and a_7=0. Here, the conditions of Eqs. (10)–(12), (15), (18), and (21) are required, and we obtain a_2=31/32, a_3=−13/16, a_4=−1/2, a_5=3/16, and a_6=1/32. The 15-frame algorithm is

$$\begin{aligned}&\tan\theta_1\\&=\frac{127(I_1-I_{-1})-99(I_3-I_{-3})+29(I_5-I_{-5})-(I_7-I_{-7})}{120(I_2+I_{-2})-64(I_4+I_{-4})+8(I_6+I_{-6})-128I_0}.\end{aligned} \quad (22)$$

The phase-restoration error function $\Delta\theta_1$ of the 15-frame algorithm can be expressed as

$$\Delta\theta_1=\frac{\varepsilon^8}{256}\sin(2\theta_1). \quad (23)$$

From Eqs. (14), (17), (20), and (23), we can find that the phase-restoration error achieves its maximum in the initial phase of π/4. Phase-restoration errors for different phase-shifting algorithms are shown in Fig. 2, where the initial phase is assumed to be π/4. With the same phase-shifting error, the phase-restoration error is smaller as more frames are used.

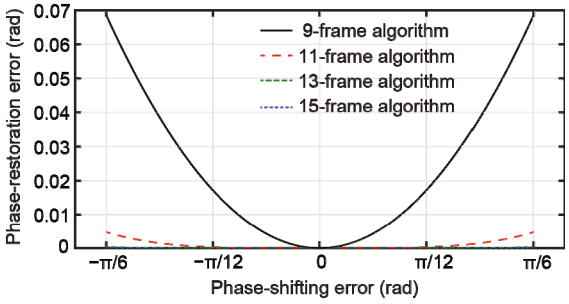

Fig. 2 Phase-restoration error with different algorithms

4 Optimized algorithms focusing on the zeroth-order effect

In case of priority optimization of the zeroth-order effect, the constant terms in A_1 are set to equal

those in B_1 (Eq. (12)). The zeroth-order effect is compensated for with the phase-shifting algorithm. The constant terms in A_2, A_3, B_2, and B_3 are assumed as zeros, which are the conditions of Eqs. (10) and (11). The 9-frame algorithm solved from Eqs. (10)–(12) is the same as that solved from Eq. (13).

4.1 New 13-frame phase-shifting algorithm

For a larger zeroth-order effect error, let the terms of ε in A_2, A_3, B_2, and B_3 be zeros. The conditions are

$$\sqrt{2}\left(\frac{3}{2}a_3+\frac{5}{2}a_5-\frac{7}{2}a_7-\frac{1}{2}a_1\right)=0, \tag{24}$$

$$6a_6-2a_2=0. \tag{25}$$

When 13 interferogram frames are used, we obtain a_1=1 and a_7=0. Here, we let the conditions of Eqs. (10)–(12), (24), and (25) be satisfied. Therefore, we obtain a_2=3/4, a_3=−1/2, a_4=−1/2, a_5=1/2, and a_6=1/4. The new 13-frame algorithm is

$$\tan\theta_1=\frac{4(I_1-I_{-1})-2(I_3-I_{-3})+2(I_5-I_{-5})}{3(I_2+I_{-2})-2(I_4+I_{-4})+(I_6-I_{-6})-4I_0}. \tag{26}$$

The new 13-frame algorithm eliminates constant terms and the terms of ε in A_2, A_3, B_2, and B_3, while the 13-frame algorithm eliminates only constant terms. So, the ability to compensate for the zeroth-order effect error of the new 13-frame algorithm is better than that of the original 13-frame algorithm.

4.2 Simulation

The procedures of lateral shearing interference and phase-restoration with the zeroth-order effect are simulated to verify the analysis in Section 4.1. In the simulation, a wavefront with 0.5λ spherical aberration is located in the unit circle. The wavefront is sheared in the x direction, and the shearing ratio is assumed as 0.1. The zeroth-order effect is V_2=V_3=10%V_1.

The 9- and 13-frame interferograms are obtained with 9 and 13 phase-shifting steps, respectively. The phase-shifting amount is π/2 and the phase-shifting error is π/16. The phase-restoration errors with the 9- and 13-frame algorithms are shown in Figs. 3a and 3b, respectively. From these two figures, we see that the maximum absolute value of the restoration error of the 9-frame algorithm is larger than 0.04 rad with a large zeroth-order effect error, while that of the 13-frame algorithm is smaller than 0.007 rad. The restoration accuracy of the new 13-frame algorithm is higher than that of the 9-frame algorithm.

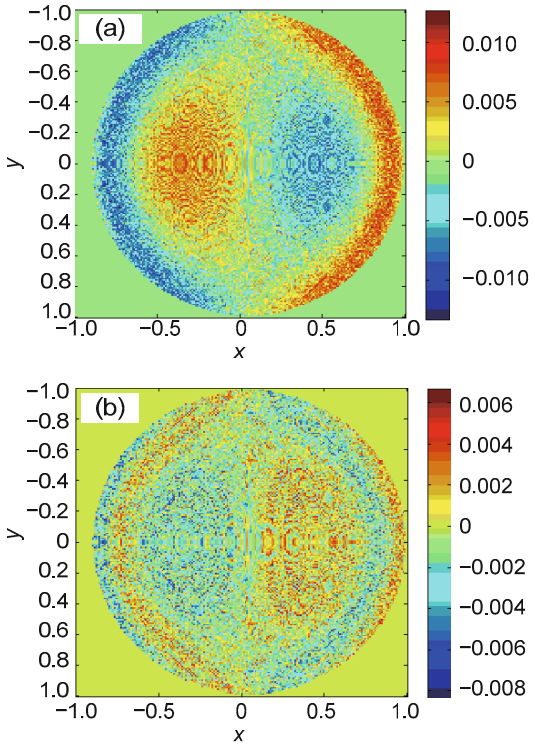

Fig. 3 Phase-restoration error with the 9-frame algorithm (a) and the new 13-frame algorithm (b)

For different zeroth-order effect errors, the different interferograms are generated with 9 and 13 phase-shifting steps, respectively. The phase-restoration errors are obtained with the 9-frame algorithm and the new 13-frame algorithm. The restoration root mean square (RMS) errors of those algorithms are shown in Fig. 4. The phase-restoration error increases with the increasing zeroth-order effect error when using the 9-frame algorithm. The restoration RMS error of the new 13-frame algorithm changes little with the increasing zeroth-order effect error. With the same zeroth-order effect error, the restoration accuracy of the new 13-frame algorithm is higher than that of the 9-frame algorithm. The accuracy difference is remarkable, especially when the zeroth-order effect error is large.

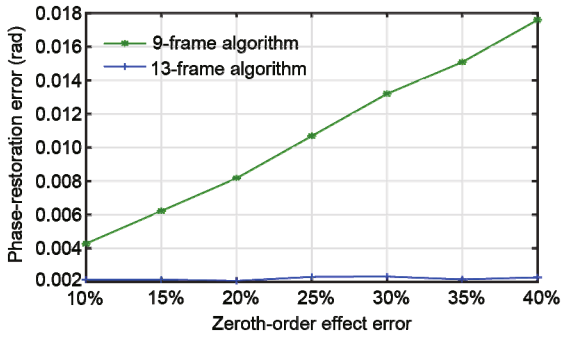

Fig. 4 Restoration root mean square errors of the 9-frame and the new 13-frame algorithms for different zeroth-order effect errors

5 Conclusions

In this paper, we have derived a general expression of phase-shifting algorithms for a grating lateral shearing interferometer and have offered a detailed design method. Based on the expression and method, a series of phase-shifting algorithms have been designed that can eliminate the phase-shifting error and the zeroth-order effect. The 9-, 11-, 13-, and 15-frame phase-shifting algorithms have been designed with the primary optimization of suppressing the phase-shifting error. The new 13-frame phase-shifting algorithm has been designed with the primary optimization of suppressing the zeroth-order effect. The analysis and simulations showed that the designed phase-shifting algorithms can eliminate effectively the phase-shifting error and the zeroth-order effect error for the grating lateral shearing interferometer. Under the condition of n>15, the algorithms can also be designed with the method introduced in this paper.

References

Bai F, Wang X, Huang K, et al., 2013. Analysis of spatial resolution and pinhole size for single-shot point-diffraction interferometer using in closed-loop adaptive optics. *Opt Commun*, 297:27-31. https://doi.org/10.1016/j.optcom.2013.01.070

Bueno JM, Acosta E, Schwarz C, et al, 2010. Wavefront measurements of phase plates combining a point-diffraction interferometer and a Hartmann-Shack sensor. *Appl Opt*, 49(3):450-456. https://doi.org/10.1364/AO.49.000450

Dai F, Li J, Wang X, et al., 2016. Exact two-dimensional zonal wavefront reconstruction with high spatial resolution in lateral shearing interferometry. *Opt Commun*, 367:264-273. https://doi.org/10.1016/j.optcom.2016.01.068

Fang C, Xiang Y, Qi K, et al., 2013. An 11-frame phase shifting algorithm in lateral shearing interferometry. *Opt Expr*, 21(23):28325-28333. https://doi.org/10.1364/OE.21.028325

Fujii T, Kougo J, Mizuno Y, et al., 2003. Portable phase measuring interferometer using Shack-Hartmann method. *Proc SPIE*, 5038:726-732. https://doi.org/10.1117/12.482699

Gao P, Harder I, Nercissian V, et al., 2010. Phase-shifting point-diffraction interferometry with common-path and in-line configuration for microscopy. *Opt Lett*, 35(5):712-714. https://doi.org/10.1364/OL.35.000712

Goldberg KA, Naulleau P, Denham P, et al., 2004. EUV interferometric testing and alignment of the 0.3-NA MET optic. *Proc SPIE*, 5374:64-73. https://doi.org/10.1117/12.546199

Hasegawa M, Ouchi C, Hasegawa T, et al., 2004. Recent progress of EUV wave-front metrology in EUVA. *Proc SPIE*, 5533:27-36. https://doi.org/10.1117/12.562431

Hasegawa T, Ouchi C, Hasegawa M, et al., 2004. EUV wave-front metrology system in EUVA. *Proc SPIE*, 5374:797-807. https://doi.org/10.1117/12.536327

Lee SH, Naulleau P, Goldberg KA, et al., 2000. Phase-shifting point-diffraction interferometry at 193 nm. *Appl Opt*, 39(31):5768-5772. https://doi.org/10.1364/AO.39.005768

Li J, Gong Y, Chen H, et al., 2015. Wave-front reconstruction with Hartmann-Shack sensor using a phase-retrieval method. *Opt Commun*, 336:127-133. https://doi.org/10.1016/j.optcom.2014.09.086

Miyakawa R, Naulleau P, Goldberg K, 2009. Analysis of systematic errors in lateral shearing interferometry for EUV optical testing. *Proc SPIE*, 7272:72721V. https://doi.org/10.1117/12.812340

Schreiber H, Schwider J, 1997. Lateral shearing interferometer based on two Ronchi gratings in series. *Appl Opt*, 36(22):5321-5324. https://doi.org/10.1364/AO.36.005321

Takeda M, Kobayashi S, 1984. Lateral aberration measurements with a digital Talbot interferometer. *Appl Opt*, 23(11):1760-1764. https://doi.org/10.1364/AO.23.001760

Wang F, Wang X, Ma M, et al., 2006. Aberration measurement of projection optics in lithographic tools by use of an alternating phase-shifting mask. *Appl Opt*, 45(2):281-287. https://doi.org/10.1364/AO.45.000281

Zhu Y, Gemma T, 2001. Method for designing error-compensating phase-calculation algorithms for phase-shifting interferometry. *Appl Opt*, 40(25):4540-4546. https://doi.org/10.1364/AO.40.004540

Zhu Y, Sugisakia K, Ouchia C, et al., 2004. Lateral shearing interferometer for EUVL: theoretical analysis and experiment. *Proc SPIE*, 5374:824-832. https://doi.org/10.1117/12.537331

Zhu Y, Sugisaki K, Okada, M, et al., 2007. Wavefront measurement interferometry at the operational wavelength of extreme-ultraviolet lithography. *Appl Opt*, 46(27):6783-6792. https://doi.org/10.1364/AO.46.006783